We are IntechOpen, the world's leading publisher of Open Access books Built by scientists, for scientists

4,800
Open access books available

122,000
International authors and editors

135M
Downloads

Our authors are among the

154
Countries delivered to

TOP 1%
most cited scientists

12.2%
Contributors from top 500 universities

CLARIVATE ANALYTICS BOOK CITATION INDEX INDEXED

WEB OF SCIENCE™

Selection of our books indexed in the Book Citation Index in Web of Science™ Core Collection (BKCI)

Interested in publishing with us?
Contact book.department@intechopen.com

Numbers displayed above are based on latest data collected.
For more information visit www.intechopen.com

Chapter 13

The Coupled Magnetic Field Effects on the Microstructure Evolution and Magnetic Properties of As-Deposited and Post-Annealed Nano-Scaled Co-Based Films — Part II

Donggang Li, Qiang Wang, Agnieszka Franczak, Alexandra Levesque and Jean-Paul Chopart

Additional information is available at the end of the chapter

http://dx.doi.org/10.5772/61349

Abstract

Superimposed external magnetic fields during electrodeposition process offers the possibility to tailor the microstructure and properties of the obtained films in a very efficient, contactless, and easily controllable way, which is caused by so-called magnetohydrodynamic (MHD) effect. On the other hand, the non-equilibrium state of as-electrodeposited nanocrystalline films provides a strong thermodynamic potential for microstructural transformation. This means that the beneficial effect of magneto-electrodeposition on a nanocrystalline film can be completely consumed by thermal exposure at a relatively low temperature. Magnetic field annealing has been confirmed to be useful for tailoring the microstructure of as-deposited nanocrystalline films for their widespread uses.

The particular interest of this book chapter, "Growth of Co-based magnetic thin films by magnetic fields (MF) assisted electrodeposition and heat treatment," is the finding that the microstructure and magnetic properties of nanocrystalline Co-based alloys and oxides like CoX (X = Cu, Ni, NiP, FeO.) are improved by imposition of MF during elaboration process or post-annealing process. According to the previous study, the targeted scientific activities pay more attention to develop alloys and oxides in nano-scale using pulsed electrodeposition assisted by high magnetic field (HMF). (Note: Since the instantaneous current density during pulse electrodeposition is higher than that during direct current plating, the microstructure of the nano-scale electrodeposits can be more easily controlled by perturbing the desorption/adsorption processes occurring in the pulse electrodeposition process).

During the experiment, high magnetic field is an in situ method for the control of electrodeposition process. The obtained material is then annealed or oxidized after elaboration under HMF. Comparative studies are performed concerning the electrodeposition process in a high magnetic field, by changing the magnetic field parameters, such as magnetic

flux density, direction, gradient. Then, we will investigate the evolution of the microstructure induced by magnetic field, and the control of crystal orientation, crystal size, and its distribution by a HMF. By comparing the microstructure and magnetic properties of the film with and without a HMF, we can find optimum magnetic field parameters for the control of the growth of nanocrystalline Co-based magnetic film. The functionality of materials could then be improved by both processes under HMF: electrodeposition and annealing.

Keywords: coupled magnetic field effects, microstructure evolution, nano-scaled Co-based films

1. Evolution of morphology in electrodeposited nanocrystalline Co–Ni alloy films by in situ high magnetic field application

1.1. Introduction

It is well known that the magnetic properties of deposits (such as GMR effect, coercivity fields, moment per atom, etc.) are strongly related to the morphology, i.e., grain shape, grain size, and layer roughness. For instance, the lower the roughness of Co–Cu multi-layers, the higher the GMR effect is visible. On the opposite, an increase in roughness of the magnetic layer leads to an increase of its coercivity fields H_c [1]. The morphology of electrodeposits is especially sensitive to mass transport and chemical reactions, which can be controlled by a magnetic field due to the Lorentz force induced by the interaction of magnetic field and current (magneto-hydrodynamic effect, MHD). Therefore, superimposing a magnetic field during electrodeposition is an interesting interdisciplinary zone, with promising opportunities for producing or tailoring novel nanocrystalline materials with better magnetic properties. For instance, as a non-contact method, magnetic field can be used for optimization of electrodeposited CoNi alloys that can be used in wireless micro-robots for biomedical applications [2].

Recently, weak magnetic field (lower than 1 T) effects on the electrodeposition process and the morphology of ferromagnetic deposits have been reported by different groups [3]. Krause et al. [4] reported that Co deposit shape changed into double-sized hexagonal crystallites, if a 1 T magnetic field was applied parallel to the surface of substrate. Ispas et al. [5] found that smaller grains and lower roughness for NiFe electrodeposits have been obtained with superimposition of a magnetic field up to 0.7 T. A similar observation of reducing the grain size and roughness in NiCu alloy with an application of a parallel-to-electrode magnetic field has been made by Tabakovic et al [6]. On the contrary, atomic force microscopy in Ref. [7] showed that a magnetic field induced an increase in the surface roughness of the Ni-layer electrodeposits. Many other experimental results highlight that the influence of magnetic field on the morphology of electrodeposits is varied between different reports, and not fully understood. Thanks to the development of superconducting technology, similar studies for electrochemical reaction with an in situ high magnetic field (HMF) application [8] can be conducted to undertake other experimental investigations in order to understand the magnetically induced effects and obtain new materials due to better control of ion transport in bath

http://dx.doi.org/10.5772/61349

and crystallization process, and in turn better control of the magnetic properties of deposits by the application of magnetic fields. In this work, we focus on the effects of HMF on the morphology of the nanocrystalline CoNi film. A clear dependence of grain shape, grain size, and layer roughness on magnetic flux density was characterized by field-emission scanning electronic microscopy (FE-SEM) and atomic force microscopy (AFM).

1.2. Experimental

All electrodeposition experiments were performed in a three-electrode cell without agitation.

ITO (1000 A) glass of 1 cm diameter was used as the working electrode, the counter electrode was a quadrate Pt plate of $1 \times 2cm$, and $Hg/Hg_2SO_4/K_2SO_4$(sat.) was used as reference electrode. The aqueous electrolyte contained 0.3 M $CoSO_4.7H_2O$ + 0.7 M $NiSO_4.6H_2O$ + 0.4 M H_3BO_3 + 0.015 M saccharin. The pH was adjusted to 4.7 by adding 1 M NaOH solution. Galvanostatical deposition, using a current density of 10 mA /cm^2 was performed at 50℃ for 1 min. A water-cooled superconducting magnet (CNRS, Grenoble, France) supplied a magnetic flux density up to 12 T, which was superimposed to the electrochemical cell during the electrodeposition process in the parallel direction to the vertical electrode surface. Surface morphology and chemical composition of the deposited films were investigated by FE-SEM appended with an energy-dispersive X-ray spectroscope (EDX, SUPRA 35, Japan) at three points of the CoNi films. The topography and the roughness were investigated with AFM (NTEGRA AURA, NT-MDT, Russia). Each sample was measured in areas of $5\mu m \times 5\mu m$ at three different positions on the film.

1.3. Results and discussion

Typical FE-SEM morphologies of CoNi films electrodeposited with different magnetic intensities up to 12T are shown in Figure 1. The figure demonstrates drastic morphological variations with the magnetic flux density (B). The short-clavated shape of the grains is similar in two cases: electrodeposition without magnetic field and with a weak magnetic field of 1 T (Figure 1. a–b). When the applied magnetic field was increasing from 3 to 12 T, nanosheets-like structures in a three-dimensional network without obvious grain boundary are clearly observed in CoNi deposits. The morphologies of these deposits are very similar to those reported in Bai. et al.'s work [9], although these authors found this kind of nanowires structure in Fe-Co deposits. The dependence of the mean diameter of these nanosheets on the magnetic flux density shows a tendency to firstly increase and then decrease. In the case of electrodeposition under superimposition of 12 T magnetic field (Figure 1 f), the mean size of the silk-like nanosheets in the film reaches a minimum with some agglomerate distributing in it, which can also be observed in Figure 1a. In addition, there is an evolution of grain shape from short-clavate in case of 0—1 T to nanosheets at 3–12 T.

Table 1 displays the magnetic field effect on CoNi film composition during the electrodeposition. It can be seen that cobalt contents in the film augmented from 70% to around 79% with the increase of B from 0 to 9 T, but decreased when the magnetic fields increased from 9 to 12 T. The dependence of Co/Ni ratio on B exhibits a similar trend as the evolution of morphology.

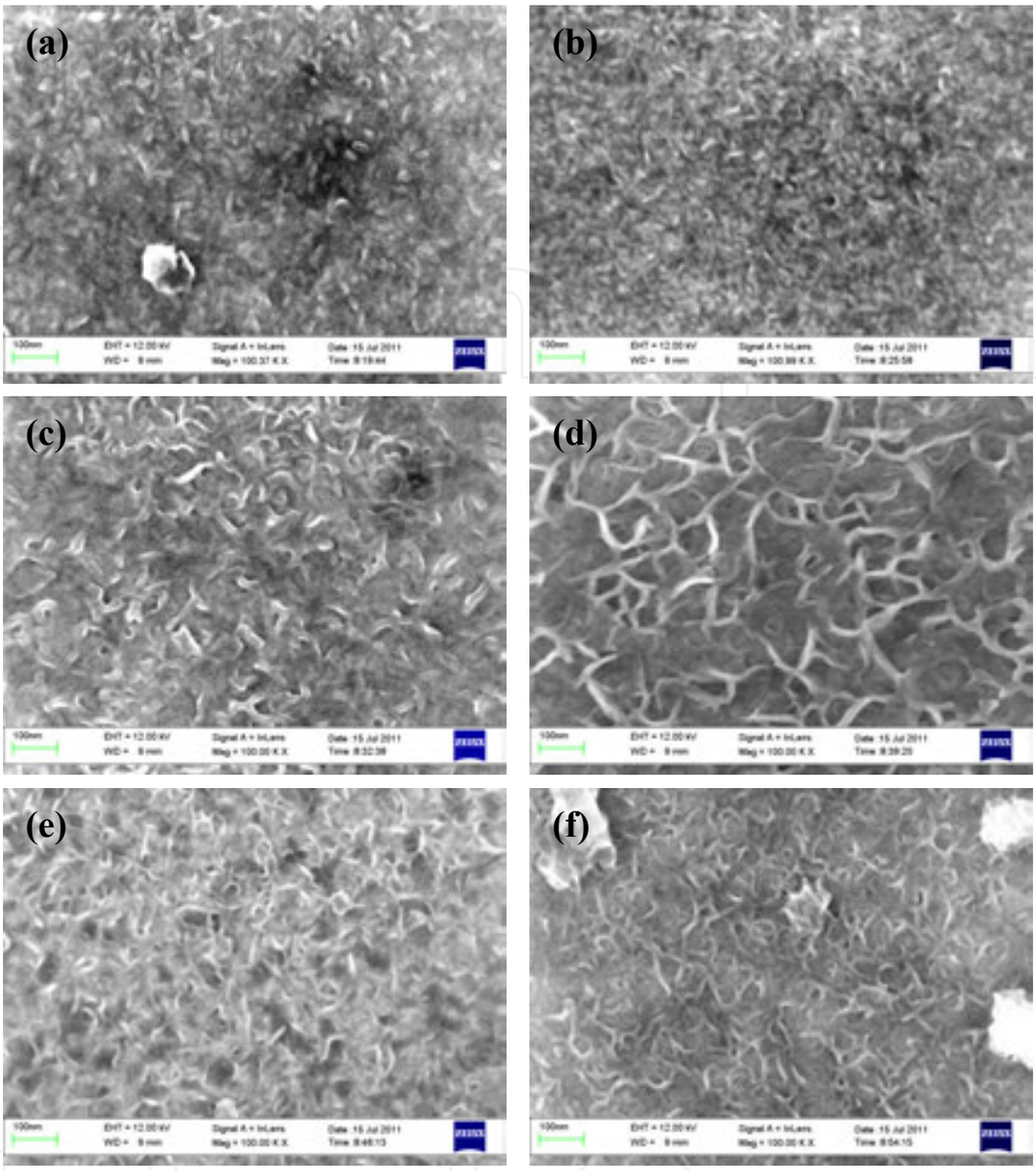

Figure 1. FE-SEM images showing the morphology of CoNi films electrodeposited with high magnetic fields of (a) 0 T, (b) 1 T, (c) 3 T, (d) 6 T, (e) 9 T, (f) 12 T.

Table 1 displays the magnetic field effect on CoNi film composition during the electrodeposition. It can be seen that cobalt contents in the film augmented from 70% to around 79% with the increase of B from 0 to 9 T, but decreased when the magnetic fields increased from 9 to 12 T. The dependence of Co/Ni ratio on B exhibits a similar trend as the evolution of morphology. To discuss the field-dependent behavior of the composition and morphology, it has to be considered that the magneto-electrochemical process is both Co (Ni) deposition and hydrogen-ion reduction at the meantime. As generally known, magnetohydrodynamic effect in a magnetic field oriented parallel to the electrode surface yields significant convection, which diminishes the diffusion layer thickness in the vicinity of electrode, and therefore increases the current efficiency. However, at high magnetic flux densities the Co deposition is diminished, since the hydrogen-ion reduction dominates the total reduction process resulting in the decrease of the current efficiencies of Co. This retarded effect is in agreement with the results obtained in the experiments of Uhlemann et al. [8] under similar conditions.

Applied magnetic field	Co (at %) in the film	Co/Ni composition ratio

http://dx.doi.org/10.5772/61349

Applied magnetic field	Co (at %) in the film	Co/Ni composition ratio
0 T	70.4 ± 0.6	2.38
1 T	76.6 ± 0.4	3.27
3 T	76.5 ± 0.6	3.26
6 T	77.4 ± 0.3	3.43
9 T	78.8 ± 0.5	3.72
12 T	76.3 ± 0.4	3.22

Table 1. Compositions of the deposited CoNi films as a function of the magnetic flux density.[16]

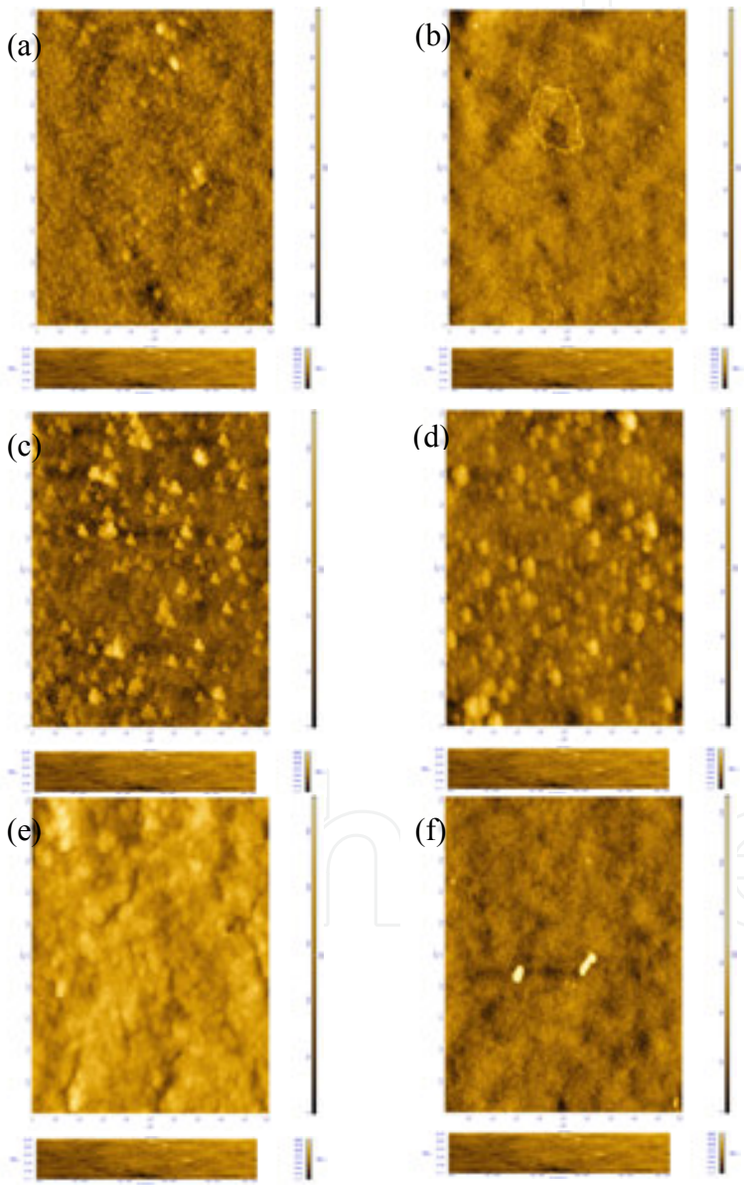

Figure 2. AFM images of top-view of CoNi films electrodeposited under high magnetic fields of (a) 0 T, (b) 1 T, (c) 3 T, (d) 6 T, (e) 9 T, (f) 12 T.

The average values of surface roughness and lateral feature size, which can be used to characterize the grain size, were calculated using standard Nova software of AFM as shown in Figure 3. AFM investigations show that the curves of the feature size and roughness exhibit non-monotonic increase up to 9 T. In contrast, feature size and roughness decreased dramatically with further magnetic field increase up to 12 T, eventually becoming smaller than

In order to quantitatively analyze the effects of HMF on grain size and roughness of the electrodeposited film, AFM top view ($5 \times 5 \mu m^2$) images of the surface topography of nanocrystalline films are shown in Figure 2. The shape and size of the grains are different in these typical samples deposited with imposed magnetic fields, being small and uniform in the case of (0–1 T); larger and irregular with accumulative cluster in the case of (3–9 T); smallest shape and more uniform in the case of 12 T. This difference indicates that the application of HMF modified the film nucleation and growth processes on the surface of cathode. It should be mentioned that the disappearance of "nanosheets" in the AFM image comparing with its existence in the SEM image is probably related to the difference in surface analysis between AFM (3D overview with the tip scanning in perpendicular to the surface) and SEM (2D morphological structure in the direction parallel to the surface).

In order to quantitatively analyze the effects of HMF on grain size and roughness of the electrodeposited film, AFM top view ($5 \times 5 \mu m^2$) images of the surface topography of nanocrystalline films are shown in Figure 2. The shape and size of the grains are different in these typical samples deposited with imposed magnetic fields, being small and uniform in the case of (0–1 T); larger and irregular with accumulative cluster in the case of (3–9 T); smallest shape and more uniform in the case of 12 T. This difference indicates that the application of HMF modified the film nucleation and growth processes on the surface of cathode. It should be mentioned that the disappearance of "nanosheets" in the AFM image comparing with its existence in the SEM image is probably related to the difference in surface analysis between AFM (3D overview with the tip scanning in perpendicular to the surface) and SEM (2D morphological structure in the direction parallel to the surface).

Figure 2. AFM images of top-view of CoNi films electrodeposited under high magnetic fields of (a) 0 T, (b) 1 T, (c) 3 T, (d) 6 T, (e) 9 T, (f) 12 T.

The average values of surface roughness and lateral feature size, which can be used to characterize the grain size, were calculated using standard Nova software of AFM as shown in Figure 3. AFM investigations show that the curves of the feature size and roughness exhibit non-monotonic increase up to 9 T. In contrast, feature size and roughness decreased dramatically with further magnetic field increase up to 12 T, eventually becoming smaller than in the case without magnetic field. It must be pointed out that the mean grain size obtained here based on the AFM images agrees well with the calculated result by using Scherrer's formula according to the X-ray diffraction.

The average values of surface roughness and lateral feature size, which can be used to characterize the grain size, were calculated using standard Nova software of AFM as shown in Figure 3. AFM investigations show that the curves of the feature size and roughness exhibit non-monotonic increase up to 9 T. In contrast, feature size and roughness decreased dramatically with further magnetic field increase up to 12 T, eventually becoming smaller than in the case without magnetic field. It must be pointed out that the mean grain size obtained here based on the AFM images agrees well with the calculated result by using Scherrer's formula according to the X-ray diffraction.

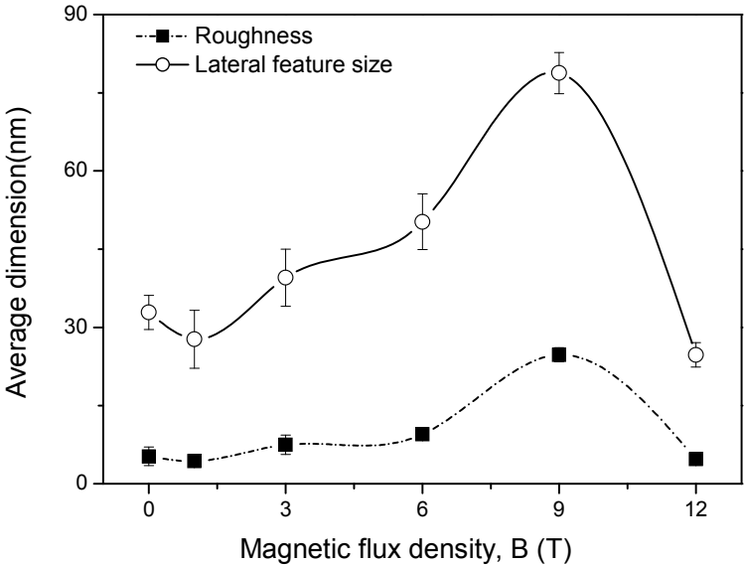

Figure 3. The dependence of roughness and grain size of CoNi films on the magnetic flux density.

The main focus of this short communication is high magnetic field effects on the electrodeposition of CoNi alloy. As regards deposition rate, the effect is observed in the mass transport limited regime [10], where the magnetic field influences the diffusion of the ions toward the cathode, but not the redox reaction. The results can be discussed by the overlapping effects of two types of force under a HMF in the direction parallel to the surface of cathode. One is the

http://dx.doi.org/10.5772/61349

Lorentz force given by $F_L = q(E + v \times B)$ (where, q is the electrical charge of an ion, E is the electrical field vector, v is the velocity of ions in electrolyte), which is responsible for a macro-MHD to decrease the thickness of the diffusion layer near the electrode, and in turn to improve the current efficiency of deposition. Whereas, at high fields the other paramagnetic force has to be taken into account, given by $F_m = \chi_m B^2 \vec{\nabla} c / 2\mu_0$ (where, χ_m is the molar susceptibility of the ions, c is the molar concentration, μ_0 is the permeability of free space), which causes paramagnetic ions to move in the direction of concentration gradient. In other words, the mass transport from electrolyte to the surface of cathode is modified by the paramagnetic force, which is in a perpendicular direction to the magnetic field. Firstly, the force acts near the edge of the electrode due to the concentration gradient in the applied magnetic field. Secondly, it acts on the whole electrode surface most likely combining with the gravitational effect and the secondary effect of the Lorentz force on the concentration profile. According to the estimation of Coey et al. [11], the value of paramagnetic force acting in aqueous electrolytes is of order 10^4(N/m^3) with a field of 1 T. Therefore, a dramatic increase of F_m in a 12 T magnetic field up to about 10^6(N/m^3), which has a magnitude comparable to that of the Lorentz force, changes the mass transport regime, and then the deposit morphology.

Obviously, the combined effects of these forces, depending on the magnetic field amplitude, cannot be discriminated in a simple way. Adsorption phenomena of ionic species and hydrogen evolution have to be regarded as very important reactions that govern the deposition process. The magnetic convection can dramatically modify these two reactions, changing the local pH and therefore texture and morphology of the deposits [12].

The present work paves the way for optimized electroplated alloys, which have been far found the most utility in micro/nano electro mechanical systems (MEMS/NEMS). These MEMS devices such as microactuators, mocrorobots, sensors, require excellent magnetic properties for actuated wirelessly by application of external magnetic fields. From the morphological viewpoint, the magnetic properties depend not only on the chemical position but also strongly on the grain size and roughness [13]. Therefore, the in situ application of high magnetic field during the electrodeposition is exceptionally well suited for tailoring the magnetic properties of Co-based magnetic alloy for MEMS applications, by non-contact controlling compositions, grain shape, grain size and roughness.

1.4. Conclusion

The influence of a parallel (with respect to the surface of the working electrode) high magnetic field on the morphology of electrodeposited CoNi film has been investigated. The FE-SEM figures demonstrated that magnetic field induced drastic morphological variations from short-clavated grain shape to silk-like nanowires. Applied magnetic fields led to an increase of the Co/Ni atomic ratio in the deposits. AFM characterization showed that the grain size and the surface roughness firstly increased with increasing magnetic flux density (0–9 T) and then decreased (9–12 T). The non-monotonic dependence of morphology on magnetic flux density could be explained by the overlapping of cumulative effects of Lorentz force on the current efficiency and of paramagnetic force on the mass transport during the electrodeposition

process that induces no obvious modifications on ionic adsorption, hydrogen evolution, and local pH.

Note: The main part, figures, and tables in this **Section 1** have been published in Ref., as Li D, Levesque A, Franczak A, Wang Q, et al. Talanta 2013;110(15):66–70.

2. Growth and magnetic properties of the Co–Cu/Cu films electrodeposited under high magnetic field

2.1. Introduction

During the past few years, a great interest was focused on the Co–Cu alloys, mainly because of their applications in magnetic sensing devices. It has been shown that due to the modifiable magnetic characteristics of deposited Co–Cu films, it is possible to obtain some desired properties of this system suitable for sensor applications [14]. Moreover, the Co–Cu alloys are ideal candidates to study the giant magnetoresistance phenomenon (GMR), which can be applied for magnetic recording and in micro-switching devices [15]. The heterogeneous Co–Cu films were usually prepared by physical vapor deposition techniques [16], while the electrodeposition one has been demonstrated useful to prepare films consisting of a metastable solid solution [17-18]. However, the composition and properties of the films are highly dependent on the deposition parameters, irrespective of the production methods.

In electrodeposition, the growth mechanism, morphology, microstructural and magnetic properties of the films depend on electrolyte pH [19], deposition potential or current density [20], intensity of agitation [21], to-be-deposited type of substrate [22], etc.. The morphology of electrodeposited metals is determined by the interplay of various atomistic phenomena occurring in electrocrystallization, in particular, the transport of ions toward the electrode and the dynamics of surface processes [23]. The establishment of a correlation between these phenomena and the formation of morphology is important in order to control film microstructure by monitoring the deposition parameters. It has been recently shown that a superimposition of an external magnetic field during electrodeposition process offers the possibility for tailoring microstructure and properties of the obtained films, what is caused by so-called magnetohydrodynamic (MHD) effect [24]. This effect is mainly considered to influence the ion transport and diffusion process in the electrolyte. Simultaneously, the growth processes of electrodeposited films are affected and changes in the microstructure of deposited films under magnetic electrodeposition conditions are observed [25].

Electrolytic growth of metals differs from other methods, providing the possibility of depositing films with structures different from those formed from the vapor phase. The electrochemical deposition is frequently characterized as a non-equilibrium material processing. Using the non-equilibrium conditions for metallurgic, inorganic, and organic crystal growths, the dendritic patterns can be observed [26]. Dendrite growth is one of the natural phenomena and fundamental of processing materials. During these growths, hierarchical structures consisting of main stems and many side branches are formed. Metallic dendrites are an

http://dx.doi.org/10.5772/61349

important class of materials, and they are attractive due to their high surface-area-to-volume ratios and their high degrees of connectivity. These properties are useful for a number of applications, including catalysis [27].

Up to the date, many of the works considering dendritic structure of deposited films get dealed with their formation influenced by the electrodeposition parameters (pH, metallic ion concentration, electrolyte temperature) rather than the influence of a high magnetic field. It is expected that dendrite growth may change its behaviour when depositing under magnetic field conditions and a superimposed B-field may present a new effect on the material performance. It is also believed that it is important to study the bahavior of Co–Cu films electrodeposited under superimposed magnetic field for production of potential sensor applications that properties can be controlled by the deposition parameters. Thus, in this study the compositional, morphological, structural, and magnetic properties are investigated as a function of applied external high magnetic field. It is observed that the changes in the film properties might have come from the variation of Co:Cu ratio in the films produced under magnetic conditions.

2.2. Experimental method

The electrochemical experiments were performed in a conventional three-electrode cell. The working electrode (WE) was a glass substrate of a square size of 10 × 10 mm and 1.1 mm height, covered with ITO (In_2O_3:SnO_2) coating (electric contact layer) and embedded into a cylindrical holder. The counter electrode was made of a platinum plate and the reference electrode was a saturated mercury sulphate electrode (SSE). Electrodeposition process has been carried out in a cylindrical double-wall cell under the conditions listed in Table 2. The electrochemical cell was plunged into the gap of Drusch EAM 20G electromagnet that delivers a uniform horizontal magnetic field parallel or perpendicular to the electrode surface.

Deposit	Chemical agent	Concentration mol/L	Solution pH	Solution temperature, *oC*	Current density, mA/cm^2	Depositon time, *sec*	Magnetic field, *T*
Cu seed layer	$CuSO_4.6H_2O$	0.03	4	50	–20	5	0
	H_3BO_3	0.4					
Co–Cu film	$CoSO_4.7H_2O$	0.4	4	50	–20	60	≤12
	$CuSO_4.6H_2O$	0.03					
	H_3BO_3	0.4					

Table 2. Processing conditions of electrodeposition of the Co–Cu/Cu films.

The electrodeposition process included two steps that were related to: firstly – deposition of Cu seed-layer directly onto ITO/glass substrate in order to improve deposit adherence, secondly – deposition of Co–Cu proper layer. The Cu seed-layer deposition was undertaken without an applied magnetic field, while the Co–Cu layers deposition was performed under

film	H_3BO_3	
		0.4

Table 2. Processing conditions of electrodeposition of the Co–Cu/Cu films.

The electrodeposition process included two steps that were related to: firstly – deposition of Cu seed-layer directly onto ITO/glass substrate in order to improve deposit adherence, secondly – deposition of Co–Cu proper layer. The Cu seed-layer deposition was undertaken without an applied magnetic field, while the Co–Cu layers deposition was performed under the superimposition of magnetic field with the strength up to 12 T in parallel-to-electrode surface orientation. The electrolyte pH was adjusted to proper level by addition of sulfuric acid. All of the electrochemical investigations were carried out using the chronopotentiometry method, where a constant current density was applied. The potential of the working electrode was controlled by means of a potentiostat-galvanostat VersaSTAT 4. Bruker D8 Advance has been employed to obtain X-ray diffraction patterns using standard θ–2θ geometry. Morphology of the obtained coatings has been investigated by scanning electron microscopy HITACHI SU-70 and the chemical composition has been determined by WD-XRF. The hysteresis loops have been measured by means of a vector VSM at room temperature and the magnetic field has been applied in the film in-plane configuration.

2.3. Results and discussion

2.3 Results and discussion

2.3.1 Film growth

Figure 4 represents the X-ray diffraction patterns of electrodeposited Co–Cu/Cu films with and without a superimposed high magnetic field. The diffractograms indicate the polycrystalline nature of deposited films.

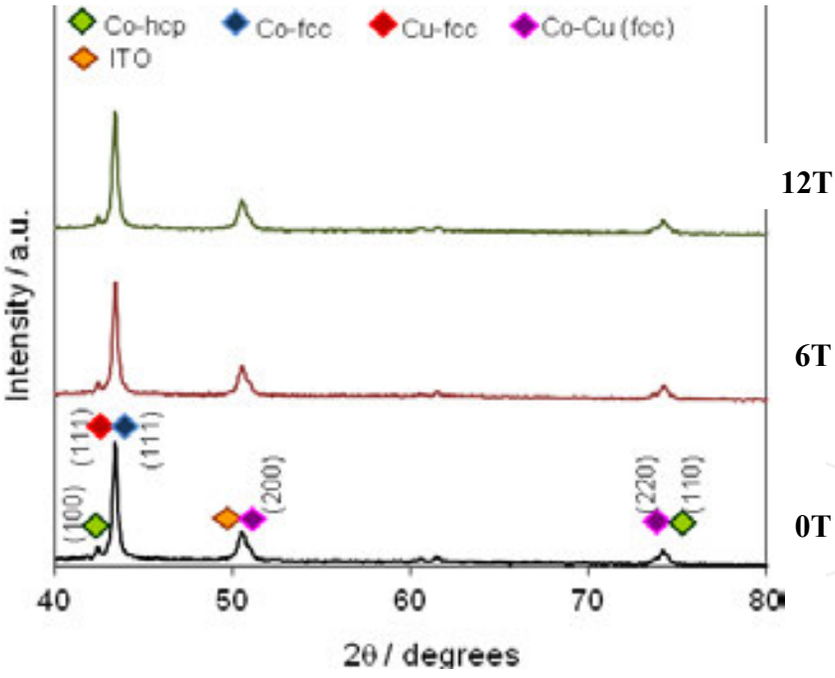

Figure 4. X-ray diffraction patterns of electrodeposited Co–Cu/Cu films with and without a superimposed magnetic field.

Though the hexagonal centered-packed structure is the most stable phase of bulk cobalt up to 420°C, experimental data reveal the coexistence of both fcc and hcp phases of Co in all Co–Cu/Cu samples. Both phases are closed-packed structures that differ only in the stacking sequence of atomic planes in the cubic (111) direction. Low activation energy for formation of stacking faults could easily lead to formation of both phases in the samples. These phase transition phenomena are also observed in electrodeposited Co–Ni powders of dendritic structure reported in [28]. The lattice parameters (a_o) extracted for Co–Cu/Cu films are formed to be very close (3.61–3.55 Å) to each

faults could easily lead to formation of both phases in the samples. These phase transition phenomena are also observed in electrodeposited Co–Ni powders of dendritic structure reported in [28]. The lattice parameters (a_o) extracted for Co–Cu/Cu films are formed to be very close (3.61–3.55 Å) to each other and are between fcc copper (3.614 Å) and fcc cobalt (3.544 Å). This confirms the formation of Co–Cu solid solution phase. Therefore, the presence of hcp Co may suggest that the Co atoms exist within the CoCu solid solution matrix, as reported in [29-30]. A superimposed high magnetic field does not bring about any phase compositional changes in the deposited films. The X-ray diffraction patterns corresponding to the other Co–Cu/Cu samples deposited under magnetic field conditions were similar. However, the SEM investigations shown in Figure 5 reveal some interesting morphological changes under superimposed high magnetic field.

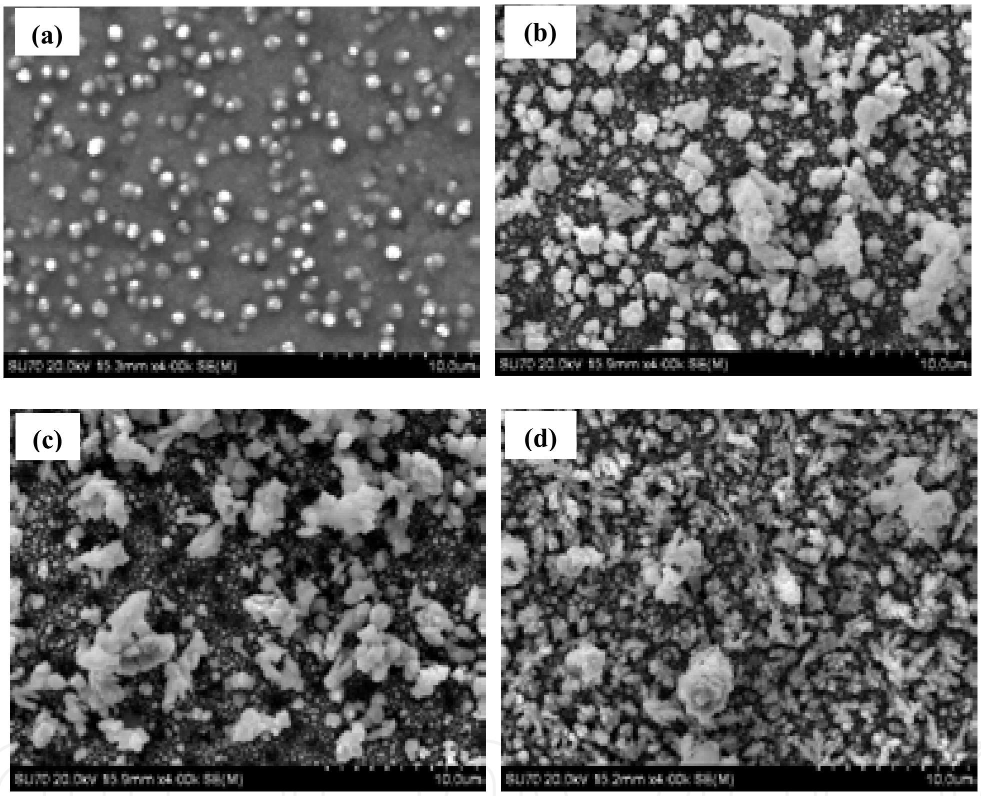

Figure 5. SEM images of electrodeposited Co–Cu/Cu films under magnetic field conditions of: (a) –0 T, (b) –6 T, (c) –9 T, (d) –12 T.

Figure 5. SEM images of electrodeposited Co–Cu/Cu films under magnetic field conditions of: (a) –0 T, (b) –6 T, (c) –9 T, (d) –12 T.

The micrographs indicate that the electrodeposited Co–Cu/Cu alloy films are composed of two layers. This feature is especially well observed in the Co–Cu/Cu film deposited without an applied magnetic field (Figure 5a). The bottom layer is a compact thin film, while the surface layer consists of submicron-scale granular-like crystallites that adhere to the bottom layer. A superimposed high magnetic field during electrodeposition (Figure 5b–d) induces the growth of crystallites from both top and bottom layers, respectively. The granular-like nucleus observed at 0 T deposition begins to grow perpendicularly to the substrate surface and the branch-like structure is observed. The particles of a compact bottom layer grow as well, but not as fast as that of the top one. Under the magnetic field of 12 T (Figure 5d), a whole substrate surface is covered by well-defined and well-developed branched crystallites. Furthermore, a closer view of the Co–Cu/Cu film morphology obtained during electrodeposition under 12 T magnetic field (Figure 6) confirms the XRD observations revealing the presence of both fcc Cu and embedded into it hcp atoms of Co. As it can be seen, the Co–Cu/Cu film consisted of the parallel growth of branched features of fcc Cu and hexagonal-shaped crystallites of Co.

The micrographs indicate that the electrodeposited Co–Cu/Cu alloy films are composed of two layers. This feature is especially well observed in the Co–Cu/Cu film deposited without an applied magnetic field (Figure 5a). The bottom layer is a compact thin film, while the surface layer consists of submicron-scale granular-like crystallites that adhere to the bottom layer. A superimposed high magnetic field during electrodeposition (Figure 5b–d) induces the growth of crystallites from both top and bottom layers, respectively. The granular-like nucleus observed at 0 T deposition begins to grow perpendicularly to the substrate surface and the branch-like structure is observed. The particles of a compact bottom layer grow as well, but

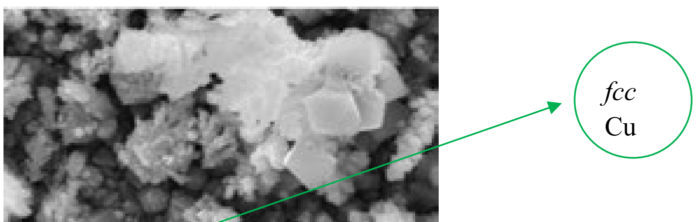

The micrographs indicate that the electrodeposited Co–Cu/Cu alloy films are composed of two layers. This feature is especially well observed in the Co–Cu/Cu film deposited without an applied magnetic field (Figure 5a). The bottom layer is a compact thin film, while the surface layer consists of submicron-scale granular-like crystallites that adhere to the bottom layer. A superimposed high magnetic field during electrodeposition (Figure 5b–d) induces the growth

not as fast as that of the top one. Under the magnetic field of 12 T (Figure 5d), a whole substrate surface is covered by well-defined and well-developed branched crystallites. Furthermore, a closer view of the Co–Cu/Cu film morphology obtained during electrodeposition under 12 T magnetic field (Figure 6) confirms the XRD observations revealing the presence of both fcc Cu and embedded into it hcp atoms of Co. As it can be seen, the Co–Cu/Cu film consisted of the parallel growth of branched features of fcc Cu and hexagonal-shaped crystallites of Co.

5d), a whole substrate surface is covered by well-defined and well-developed branched crystallites. Furthermore, a closer view of the Co–Cu/Cu film morphology obtained during electrodeposition under 12 T magnetic field (Figure 6) confirms the XRD observations revealing the presence of both fcc Cu and embedded into it hcp atoms of Co. As it can be seen, the Co–Cu/Cu film consisted of the parallel growth of branched features of fcc Cu and hexagonal-shaped crystallites of Co.

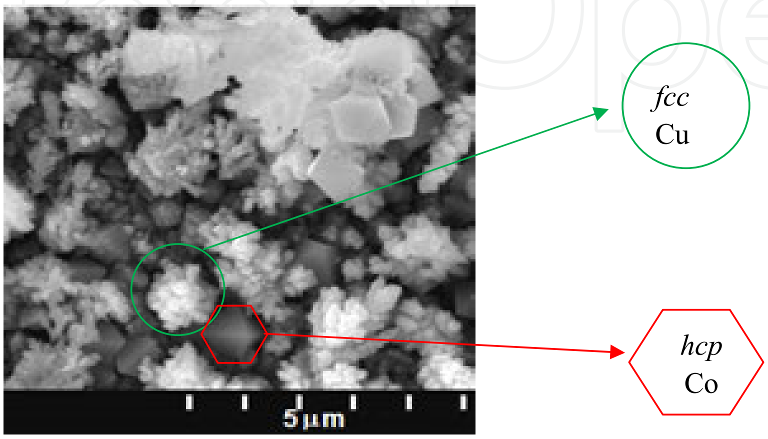

Figure 6. SEM image of the Co–Cu/Cu film electrodeposited at 12 T magnetic field, indicating the privilege growth of fcc Cu crystallistes and embedded into it some hcp atoms of Co.

Thus, the experimental results show that the surface morphology is strongly dependent on a superimposed magnetic field, more exactly by the concentration of each ions affected by an external magnetic field. With the increase of magnetic flux density, the amount of the Cu atoms in the film increased, while that of the Co atoms decreased. (Figure 7).

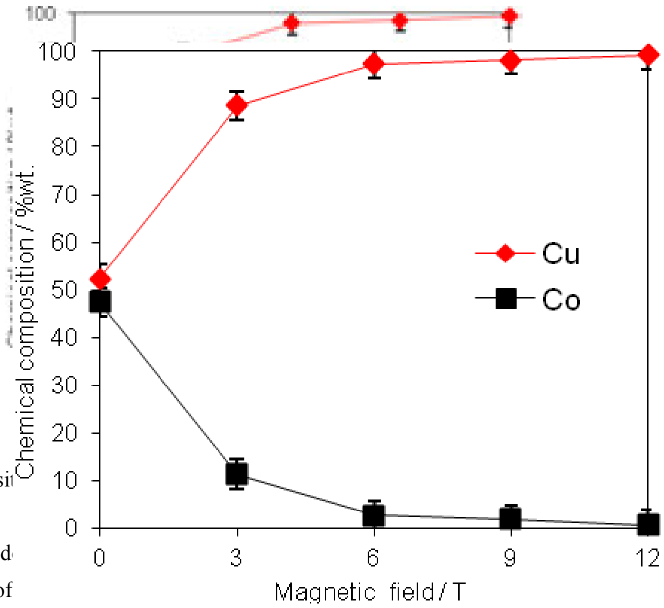

Figure 7. Chemical composit ... conditions.
In the non-magnetic electrod ... ach element, 49 wt% of Co and 51 wt% of ... wn to 1 wt%

Figure 7. Chemical composition of electrodeposited Co–Cu/Cu films under non-magnetic and magnetic conditions.

http://dx.doi.org/10.5772/61349

In the non-magnetic electrodeposition, the Co–Cu/Cu films are composed of almost equal amount of each element, 49 wt% of Co and 51 wt% of Cu. Under high magnetic field conditions, the content of Co decreases down to 1 wt% at 12 T magnetic field with simultaneous increase of Cu content up to 99 wt%. Thus, the surface morphology is strongly influenced by the Cu to Co ratio and changes from the individual particles to submicron-scale branched form, as indicated by SEM images. Therefore, the dendritic-like growth of electrodeposited Co–Cu films containing relatively high amount of Cu may be attributed to short-range crystalline order and diffusive growth of Cu as reported in Refs. [31]. It can be assumed then that a strong growth of (111) plane under magnetic conditions of electrodeposition is assigned to the diffusive growth of fcc Cu structure.

The observed effects of a superimposed magnetic field are due to the magnetohydro-dynamic (MHD) effect caused by a higher convection in the electrolyte, as a result of the Lorentz force [32]: $\overrightarrow{F_L} = \vec{J} \times \vec{B}$, which is a product of the current density flowing perpendicularly to the magnetic field. From the experimental results, it can be found that the dendrite-like forms were disordered and spacing between them became larger due to the application of the B-field, what is especially well observed during deposition at 6, 9, and 12 T magnetic field (Figure 5b–d). These phenomena clearly indicated the existence of rather intense convection during dendritic-like form growth, which has been also reported in [33]. This convection not only increases the transport of Cu and Co ions toward electrode surface but also the rate of hydrogen evolution (HER) is increased as well, affecting the deposit growth. The presence of hydrogen bubbles may be clearly seen in Figure 2d, where the presence of black holes in the bottom layer can be visible. The action of HER is recognized as a hydrogen gas bubble stirring that charges the hydrodynamic conditions as well as mass transfer in the vicinity of electrode. Hydrodynamic conditions play an important role in determining the final morphology of electrodeposits. This is mainly because as the transport of cations becomes diffusion-limited, the concentration of ions at the cathode becomes zero, leading to instability and triggering the formation of dendrite-like branched forms. Thus, as the first step the Co–Cu layer is formed with a deposition at the fewer surface steps acting as nuclei. A flow of the metal ions to the growing dendritic-like forms is localized and leads to the coalescence of hydrogen bubbles. The high local current densities concentrated around the bubbles due to their non-conductivity causes faster growth of finer crystallites. The microscopic current distribution is changed due to the adsorption of hydrogen bubbles enhanced by a magnetic field. As a final result, the current density distribution and coalescence of hydrogen bubbles create well-defined branched-like structures of different length scales. It is also assumed that dendrite crystals have a higher surface free energy compared to the equilibrium shape of the crystal and are, therefore, thermodynamically unstable compared to the latter. The origin of the dendrite therefore results from the kinetics of crystal growth under the condition where coupling between the surface phenomena (charge-transfer reactions or crystal-growth process) and the bulk transport in fluid phase occur in the system [34]. Moreover, the effect of a superimposed external high magnetic field on the morphology of electrodeposited Co–Cu/Cu alloy films seems to be a very interesting method, regarding on the possibility of electrodeposition of multilayer films, just by applying external B-field during the process.

2.3.2. Magnetic properties

Figure 8 indicates the hysteresis loops of Co–Cu/Cu alloy films electrodeposited with and without a superimposed magnetic field, measured in-the-film-plane at room temperature. It can be clearly seen that it is harder to magnetise the Co–Cu/Cu film grown under superimposed magnetic field. The Co–Cu/Cu films electrodeposited under 0 and 1 T are saturated more easily when compared to the film deposited under 3 T magnetic field, which has more inclined magnetization curve. This may indicate a more disordered arrangement of the Co atoms and, therefore, less degree of ferromagnetic order in the samples deposited under 3 T magnetic field. Furthermore, the coercive field increases for the Co–Cu/Cu samples electrodeposited under magnetic field from 110 Oe at 0 T, up to 200 Oe for the film deposited at 3 T, respectively. This value is in agreement with those usually found in Co–Cu based granular alloys with Co-rich clusters larger than 10 nm [35] and with the Co–Cu alloy containing 15 wt% of Co reported by Gomez et al. [36]. The observed magnetic behavior may be attributed then to the change of Cu:Co ratio in the Co–Cu/Cu film that is caused by the magnetic electrodeposition conditions.

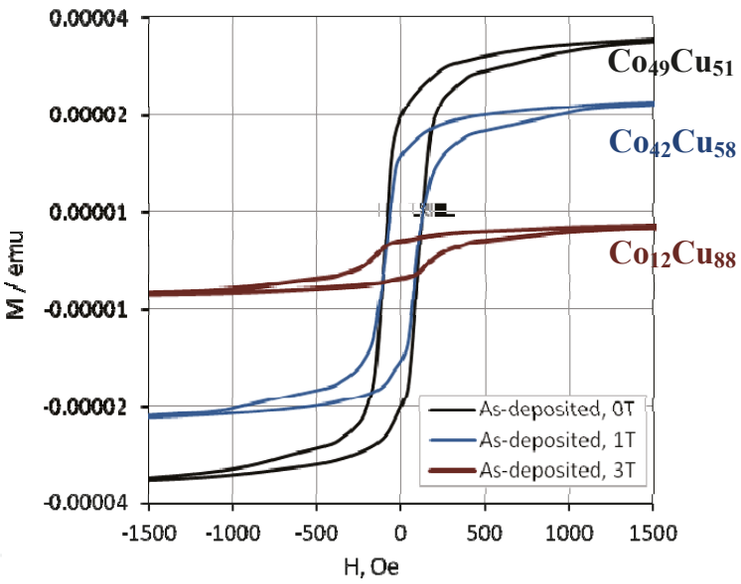

Figure 8. Magnetic behavior of the Co–Cu/Co films electrodeposited with and without a superimposed magnetic field.

When the electrodeposition process is carried out without an applied magnetic field, the chemical composition of Co–Cu/Cu film is almost equal for each Co and Cu element. A superimposed magnetic field enhances the deposition rate of copper ions, suppressing that of cobalt. Thus, the Co–Cu/Cu films consist mainly of copper crystallites (88 wt%) with low incorporation of cobalt nucleus (12 wt%), which has been already shown in the X-ray diffraction patterns (Figure 4) and confirmed by SEM analysis (Figure 5). Moreover, the compositional investigations (Figure 6) have shown that in the Co–Cu/Cu samples electrodeposited under magnetic field higher than 3 T, a drastical decrease of ferromagnetic Co atoms in the films (1 wt% at 12 T) was observed. Thus, the Co–Cu/Cu films electrodeposited at 6, 9, and 12 T magnetic field were characterized as non-magnetic materials. The presented results are in

http://dx.doi.org/10.5772/61349

agreement with the compositional dependence of saturation magnetization and coercive field given by Karaagac et al. [37]. The authors presented the EDX results, which have shown that both magnetization and coercivity are strongly affected by increasing amount of non-magnetic Cu component in the film. This in turn resulted in the increased density of dendritic-like structure of deposited films. Furthermore, the observed magnetic properties of Co–Cu/Cu alloy films are in range of which they may be controlled by electrodeposition parameters, such as superimposed magnetic field, and can be potentially used in sensor technology.

2.4. Conclusion

The influence of high magnetic fields on the growth of electrodeposited Co–Cu/Cu alloy films was studied. Furthermore, the magnetic properties of electrodeposited films in dependence on their microstructure have been determined. The Co–Cu/Cu films were of polycrystalline nature that has been preserved under magnetic electrodeposition conditions. The alloy films deposited without an applied magnetic field possessed a morphology consisting of two layers: compact bottom and top one, of granular-like structure. A superimposed external magnetic field induced the growth of both layers and as a consequence, a well-developed branched structure was formed. This was associated with the increase of Cu content in the films, which rose up drastically under magnetic field conditions. Therefore, a possible explanation for the dendritic-like growth in the surface morphology of electrodpeosited Co–Cu/Cu films may be the diffusive growth of Cu and hydrogen evolution that is favored when external magnetic field is superimposed during the process. The magnetic measurement revealed that magnetic behavior of the deposited films is controlled by the film composition, mainly by the amount of non-magnetic Cu component, which varies under magnetic field conditions. Thus, the morphological and structural changes observed under magnetic electrodeposition conditions increase the surface/volume ratio in the film and enhance their shape anisotropy.

3. Microstructure evolution and magnetic properties of CoFe2O4 thin films prepared by one-step magneto-electrodeposition

3.1. Introduction

Due to their excellent electrochemical performance, higher magnetic anisotropy, and moderate saturation magnetization, iron-cobalt oxides with spinel structures have attracted considerable interests as promising candidates for modern innovative applications, such as gas sensors[38], catalysts for various reactions[39], anodes for lithium ion batteries[40], magneto-optic recording media[41]. Up to now, a variety of methods of synthesizing $Co_xFe_{3-x}O_4$ thin films have been developed including sputtering, physical vapor deposition, chemical vapor deposition, pulsed laser deposition, and electrochemical deposition [42–45]. Most of these techniques involve a two-step process, first the CoFe alloy precursors formation, and then followed by oxidation at high temperature [46]. However, the high-temperature annealing can cause unwanted reactions between the substrate and the deposited film, which affect the grain size, morphology, chemical stability, and the magnetic property [47]. It is widely accepted that the practical

application of $Co_xFe_{3-x}O_4$ thin films will depend on the capability of precisely controlling the composition, particle size, and structure during the preparation process. Magneto-electrodeposition could be an alternative method to obtain $Co_xFe_{3-x}O_4$ thin films by single-step at low temperature, with precisely controlling the ratio of Co:Fe, morphology, and microstructure, furthermore to tailor the chemical and physical properties of the films. Recently, magnetic fields are widely used to control the mass transfer processes in electrochemical cells, since under magnetic fields a Lorenz force arises, and the magnetohydrodynamics (MHD) convection governs the hydrodynamic boundary layers. Krause et al. [4] found that in electrodeposition under a 1 T magnetic field, Co deposit shape changed into double-sized hexagonal crystallites. The previous study of us also shown that magnetic fields induced drastic morphological variations in the electrodeposited CoNi films from short-clavated grain shape to silk-like nanowires, and the applied magnetic fields led to an increase of the Co:Ni ratio in the deposits. In addition, because of the higher instantaneous current density in comparison to direct current plating, pulse electrodeposition has been found to be an effective means of perturbing the adsorption/desorption processes and hence offers an opportunity of controlling the microstructure of the electrodeposits. This work presents one-step pulse-electrodeposition of Cobalt-Ferrite thin film on the Ti substrate under 1 T magnetic fields. The aim of this work is to study the evolution of composition, surface morphology, and microstructure of cobalt ferrite thin films under the condition of magneto-pulse-electrodeposition.

3.2. Experimental

All electrodeposition experiments were performed in a conventional three-electrode cell without agitation. Polished titanium of 1 cm diameter was used as the working electrode, the counter electrode was a quadrate Pt plate of $1\times1cm$, and $Ag/AgCl/KNO_3$(sat.) was used as a reference electrode. The electrolyte was composed of 100 mM Co^{2+}, 50 mM Fe^{3+}, 150 mM triethanolamine (TEA), and 2 M NaOH. Pulse-electrodeposition using a potentiostat-galvanostat VersaSTAT 4 was performed at 80℃. The electrochemical cell was plunged into the gap of Drusch EAM 20G electromagnet that delivers a uniform horizontal magnetic field up to 1 T parallel to the electrode surface. To deposit good-quality films, various parameters such as deposition potential, magnetic flux density, deposition time, and duty cycle etc. were optimized as shown in Table 3.

Pulse-potential $V1_{Ag/AgCl}$	Deposition time, t1	Pulse-potential $V2_{Ag/AgCl}$	Deposition time, t2	Cycles	Magnetic field
–1.17 V ~ –1.19 V	1 s	–0.95 V	4 s	300	1 T

Table 3. Processing conditions of electrodeposition of the cobalt ferrite films. [51]

The surface morphology and chemical composition of the deposited films were investigated by scanning electronic microscopy (SEM) appended with an energy-dispersive X-ray spectroscope (EDX, SUPRA 35) at three different positions on the films. The topography were investigated with atomic force microscopy (AFM). For the characterization of the microstruc-

The surface morphology and chemical composition of the deposited films were investigated by scanning electronic microscopy (SEM) appended with an energy-dispersive X-ray spectroscope (EDX, SUPRA 35) at three different positions on the films. The topography were investigated with atomic force microscopy (AFM). For the characterization of the microstructure of the films, X-Ray diffraction (XRD, Bruker D8 Advance) measurements were performed using standard θ-2θ geometry with Cu $K\alpha$ radiation.

3.3 Results and discussion

Since in case of without magnetic field, the electrodeposited films obtained under the experimental condition in this work were not adherent and covered the substrates bad, all the electrodeposition were optimized by performing in a 1 T magnetic field. Typical SEM and AFM morphologies of cobalt ferrite films pulse-electrodeposited with potential ranged from –1.17 to –1.19 $V_{Ag/AgCl}$ are shown in Figure 9.

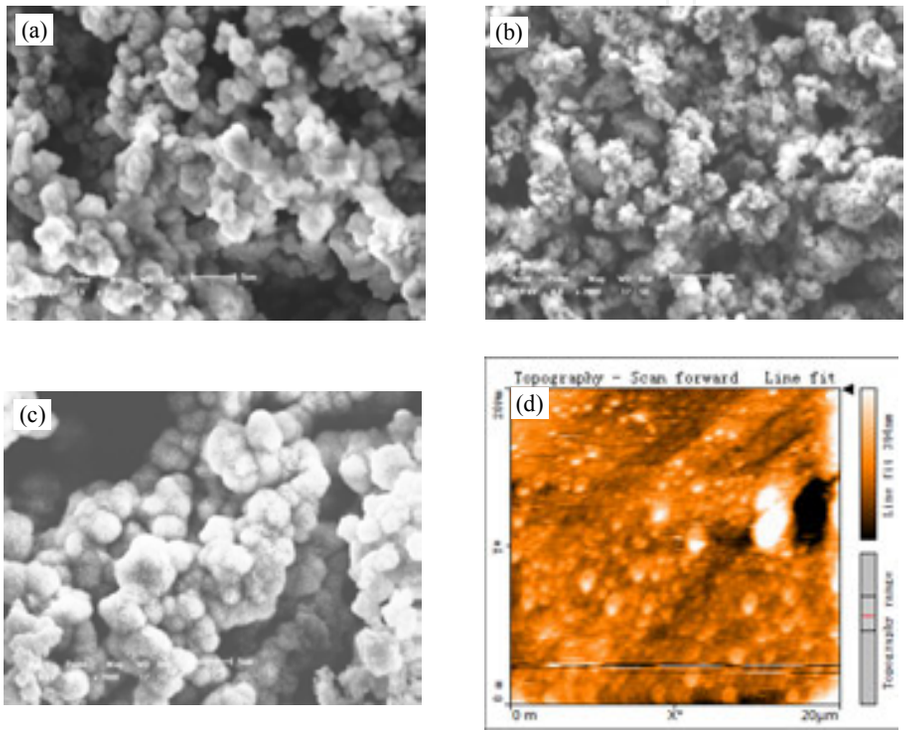

Figure 9. The SEM images of $Co_xFe_{3-x}O_4$ thin films deposited at (a) –1.17 $V_{Ag/AgCl}$; (b) –1.18 $V_{Ag/AgCl}$;(c) –1.19 $V_{Ag/AgCl}$ potentials assisted by 1 T magnetic field; and the typical AFM image of its at (d) –1.18 $V_{Ag/AgCl}$.[51]

The figure demonstrates drastic morphological variations with the pulse-potential during the electrodeposition process. The spherical grain linked together to form a coralliform morphology as shown in Figure 9a. While in case of the potential up to –1.18 $V_{Ag/AgCl}$, the top of the branches in coral seemed to split into many irregular small grains. With the increase of the applied potential to –1.19 $V_{Ag/AgCl}$, the grains of this coralliform deposit are very similar to the structure of sea anemones, that is, every spherical grain consisted of many crystal whiskers in it. Since the difference in surface analysis between AFM (3D overview in perpendicular to the surface) and SEM (2D morphological structure in parallel to the surface), the AFM image could not answer the morphology evolution of the films, but shown the films are composed of fairly large number of round nanometer-sized grains. The average values of lateral feature size, which can be used to characterize the grain size, were calculated according to AFM images in the following section.

Corresponding to the evolution of the morphology, we use the EDX to measure the change of composition in the deposited films with different pulse-potentials. The results in Table 4 have shown that the Co:Fe ratio depended on the deposition potential. The Co concentrations in the films were lower at less negative potentials and higher at more negative potentials. With the deposition potential that went to more negative values, more Co^{2+} were reduced at the electrode surface, resulting in an increase of the Co:Fe ratio in the film. These phenomena may be attributed to the MHD effect in a magnetic field, which yields significant convection, and in turn increases the current efficiency. However, due to the different kinetic reaction rate between Fe^{3+} and Co^{2+} substitution, the deviation between the Co and Fe concentration at the electrode surface was larger when the growth rate of the film was faster at more negative potentials caused by the MHD effect [48]. The deviation resulted in the Co:Fe ratio in the $Co_xFe_{3-x}O_4$ thin films a non-linear variation with the deposition potential. In case of –1.18 $V_{Ag/AgCl,}$ the x value was 0.97, which indicates that the film obtained under this condition was composed of almost $CoFe_2O_4$. This can be verified in the X-ray diffraction pattern.

Pulse-potential	Co (at%)	Fe (at%)	O (at%)	x
–1.17 $V_{Ag/AgCl}$	8.6	31.1	60.3	0.65
–1.18 $V_{Ag/AgCl}$	14.2	29.9	55.9	0.97
–1.19 $V_{Ag/AgCl}$	12.1	30.5	57.4	0.85

Table 4. The dependence of the composition of $Co_xFe_{3-x}O_4$ (0<x<1) films on the deposition potentials, the x value in $Co_xFe_{3-x}O_4$ was calculated based on the Co:Fe ratio in the films.[51]

The X-ray scan of the $Co_xFe_{3-x}O_4$ films pulse-electrodeposited on titanium were shown in Figure 10. Despite of the high peaks (marked with black dots) for the substrate (Ti), the films exhibited the diffraction peaks corresponding to both the transition metal oxides (Fe_2O_3) and the spinel cobalt ferrite ($CoFe_2O_4$). At less negative potential, the film was mostly composed of Fe_2O_3; while at more negative potentials, the film was mostly composed of $CoFe_2O_4$. Especially at –1.18 $V_{Ag/AgCl}$, the said planes as (111),(220),(311),(400),(511) corresponded to the $CoFe_2O_4$. The peaks shown in Figure 10 agree well with the Co:Fe ratio measured by EDX. For example, the x value in $Co_xFe_{3-x}O_4$ films was near unit at –1.18 $V_{Ag/AgCl,}$ which implied that by adjusting the potential assisted by magnetic field, we could prepare spinel cobalt ferrite without other oxidations by one-step magneto-electrodeposition method.

Since the morphology and microstructure of the films were dramatically depended on the potential during the electrodeposition, the grain size should also be affected by the MHD effect caused by the interaction between the pulse-current with the magnetic field. We have calculated the crystallites size by use of Scherrer's equation and AFM measurement (Table 5). The particle size R_0 was estimated from AFM analysis by the following equation [49]: $R_0 = \left(\frac{A_0}{\pi N_0}\right)^{1/2}$, in which A_0 represents the AFM total image area and N_0 is the grain number. According to these two calculated methods, the obtained films consisted of different nuclei sizes due to the changing amplitude of pulse-potential. It should be mentioned that the

http://dx.doi.org/10.5772/61349

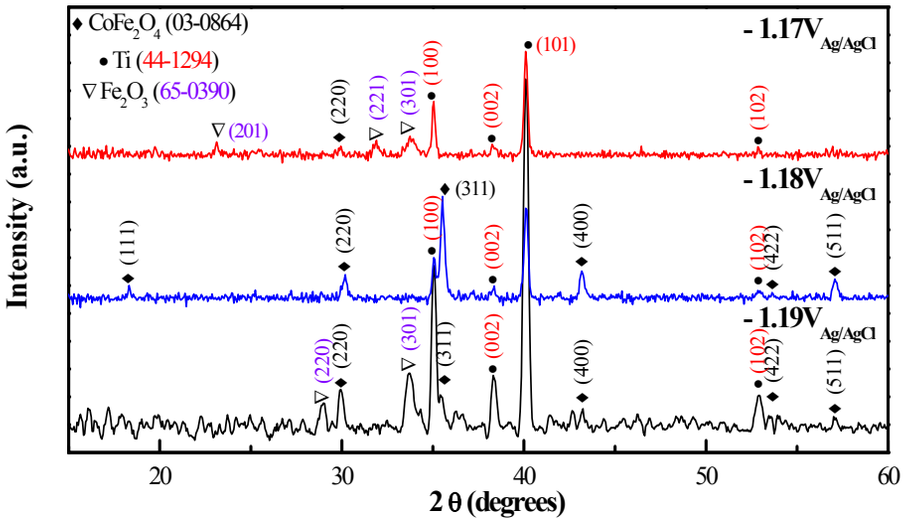

Figure 10. The X-ray diffraction pattern of cobalt ferrite films deposited at different potentials.[51]

Figure 10. The X-ray diffraction pattern of cobalt ferrite films deposited at different potentials.[51]

calculated mean grain size by using Scherrer's formula according to the X-ray diffraction share the same trend as that measured based on the AFM images. With the potential moving to more negative, the MHD effects increase to bring more $Co^{2+}(Fe^{3+})$ to the surface of the electrode, which results in the fast nucleation and is responsible for the small grain size at –1.18 $V_{Ag/AgCl}$. However, in case of –1.19 $V_{Ag/AgCl}$, the Co (Fe) deposition becomes diminished, since the hydrogen reduction dominates the total reduction process resulting in the decrease of the current efficiencies of Co (Fe). This may be a reason for the formation of bigger grain by growth at more higher pulse-potential.

Since the morphology and microstructure of the films were dramatically depended on the potential during the electrodeposition, the grain size should also be affected by the MHD effect caused by the interaction between the pulse-current with the magnetic field. We have calculated the crystallites size by use of Scherrer's equation and AFM measurement (Table 5). The particle size R_0 was estimated from AFM analysis by the following equation [49]: $R_0 = \left(\frac{A_0}{\pi N_0}\right)^{1/2}$, in which A_0 represents the AFM total image area and N_0 is the grain number. According to these two calculated methods, the obtained films consisted of different nuclei sizes due to the changing amplitude of

Potential ($V_{Ag/AgCl}$)	Sherrer (nm)	AFM (nm)
–1.17	33	47 ± 2
–1.18	25	38 ± 2
–1.19	50	61 ± 2

Table 5. Comparison of crystallites size of electrodeposited $Co_xFe_{3-x}O_4$ films obtained by calculations based on Scherrer equation and AFM.[51]

From the morphological viewpoint, the properties of the electro-deposited films depend not only on the chemical position but also strongly on the morphology, grain size, and microstructure [50]. Therefore, the in situ application of magnetic field during the pulse-electrodeposition is exceptionally well suited for tailoring the properties of cobalt ferrite, by non-contact controlling Co:Fe ratio, grain shape, grain size, and phase composition. The present work paves the way for optimized electroplated cobalt ferrite thin films by adjusting the potential during one-step magneto-electrodeposition.

3.4. Conclusion

The influence of the interaction between the pulse-potential and a magnetic field with a flux density up to 1 T on the morphology and microstructure of electrodeposited $Co_xFe_{3-x}O_4$ film

has been investigated. The SEM figures demonstrated that MHD effects induced drastic morphological variations from coral-like to sea-anemone-like. More negative potential led to an increase of the Co:Fe atomic ratio in the deposits. The XRD pattern further verified that at –1.18 $V_{Ag/AgCl}$, we could obtain $CoFe_2O_4$ film with ultra-fine grains in it by one-step magneto-electrodeposition. The non-monotonic dependence of morphology, composition, and microstructure on pulse-potential may be attributed to the overlap effects of MHD on the current efficiency and on the hydrogen-ion reduction during the deposition process.

Note: The main part, figures, and tables in this **Section 3** have been published on the 9th International Pamir Conference on Fundamental and Applied MHD, Riga, Latvia, June 16–20, 2014, Ref. [51].

Acknowledgements

This work was financially supported by the National Natural Science Foundation of China (Grant Nos. 51425401, 51101032), the Fundamental Research Funds for the Central Universities (Grant Nos. N130402002, N140902001), Agence Nationale de la Recherche France (Programme COMAGNET, Grant No. 2010-INTB-903-01). The authors would like to thank Dr. A. Levesque for her contributions about the SEM, XRD analysis, and useful discussion. The authors are also indebted to Dr. Piort Zabinski from the AGH University of Poland for his support of AFM in this work.

Author details

Donggang Li[1,3*], Qiang Wang[2], Agnieszka Franczak[3], Alexandra Levesque[3] and Jean-Paul Chopart[3]

*Address all correspondence to: lidonggang@smm.neu.edu.cn

1 School of Materials and Metallurgy, Northeastern University, Shenyang, China

2 Key Laboratory of Electromagnetic Processing of Materials (Ministry of Education), Northeastern University, Shenyang, China

3 LISM, Université de Reims Champagne-Ardenne, France

References

[1] Palasantzas G, Zhao Y-P, De Hosson JThM, Wang GC. Roughness effects on magnetic properties of thin films.Physica B 2000;283:199–202.

[2] Ergeneman O, Sivaraman KM, Pané S, Pellicer E, Teleki A, Hirt AM, Baró MD, Nelson BJ. Morphology, structure and magnetic properties of cobalt-nickel films obtained from acidic electrolytes containing glycine.Electrochim Acta 2011;56:1399–408.

[3] Msellak K, Chopart J-P, Jbara O, Aaboubi O, Amblard J. Magnetic field effects on Ni-Fe alloys codeposition. J Magn Magn Mater 2004;281:295–304.

[4] Krause A, Hamann C, Uhlemann M, Gebert A, Schultz L. Influence of a magnetic field on the morphology of electrodeposited cobalt, J Magn Magn Mat 2005;290:261–4.

[5] Ispas A, Matsushima H, Plieth W, Bund A.Influence of a magnetic field on the electrodeposition of nickel-iron alloys. Electrochim Acta 2007;52:2785–95.

[6] Tabakovic I, Riemer S, Sun M, Vas'ko VA, Kief M. Effect of magnetic field on NiCu electrodeposition from citrate plating solution and characterization of deposit.J Electrochem Soc 2005;152:C851–60.

[7] Bund A, Ispas A. Influence of a static magnetic field on nickel electrodeposition studied using an electrochemical quartz crystal microbalance, atomic force microscopy and vibrating sample magnetometry.J Electroanal Chem 2005;575:221–8.

[8] Uhlemann M, Krause A, Gebert A, Chopart J-P. Electrochemical deposition of co under the influence of high magnetic fields.J Electrochem Soc 2005;152:C817–26.

[9] Bai A, Hu C-C. Cyclic voltammetric deposition of nanostructured iron-group alloys in high-aspect ratios without using templates.Electrochem Commun 2003;5:78–82(619-624).

[10] Hinds G, Coey JMD, Lyons MEG. Magnetoelectrolysis of copper.J Appl Phys 1998;83:6447–9.

[11] Coey JMD, Hinds G.Magnetic electrodeposition. J Alloys Compd 2001;326:238–45.

[12] Uhlemann M, Krause A, Gebert A.Effect of a magnetic field on the local pH value in front of the electrode surface during electrodeposition of Co. J Electroanal Chem 2005;577:19–24.

[13] Armyanov A. Electrochim Acta 2000;45:3323–35.

[14] Sun B, Yang ZT, Zou XW, Jin ZZ.Nonequilibrium microstructure of Pb-Sn alloy obtained from electrochemical deposition. Mater Chem Phys 2004;86:144–9.

[15] Nabiyouni G, Schwarzacher W, Rolik Z, Bakonyi I. Giant magnetoresistance and magnetic properties of electrodeposited Ni-Co-Cu/Cu multilayers.J Magn Magn Mater 2002;253:77–85.

[16] Berkowitz AE, Mitchell JR, Carey MJ, Young AP, Zhang S, Spada FE, Parker FT, Hutten A, Thomas G. Phys Rev Lett 1992;68:3745.

[17] Gomez E, Llorente A, Alcobe X, Valles E. Electrodeposition for obtaining homogeneous or heterogeneous cobalt-copper films.J Solid State Electrochem 2004;8:82–8.

[18] Fan X, Mashimo T, Huang X, Kagayama T, Chiba A, Koyama K, Motokawa M. Magnetic properties of Co-Cu metastable solid solution alloys.Phys Rev B 2004;69:094432.1–094432.6.

[19] Liu QX, Min JH, Cho JU, Kim YK.The pH dependence of Co-Cu alloy thin films fabricated on amorphous substrate by DC electrodeposition. IEEE Trans Magn 2005;41(2):930–2.

[20] Karaagac O, Alper M, Kockar H. Characterisations of CoCu films electrodeposited at different cathode potentials.J Magn Magn Mater 2010;322:1098–101.

[21] Lopez Anton R, Fdez-Gubieda ML, Garcia-Arribas A, Herreros J, Insausti M. Preparation and characterisation of Cu-Co heterogeneous alloys by potentiostatic electrodeposition.Mat Sci Eng A 2002;335:94–100.

[22] Karaagac O, Kockar H, Alper M. Composition Dependence of Structural and Magnetic Properties of Electrodeposited Co-Cu Films.IEEE Trans Magn 2010;46(12):3973–7.

[23] Lopez Anton R, Fdez-Gubieda ML, Insausti M, Garcia-Arribas A, Herreros J. Influence of the preparation method on the properties of Cu-Co heterogeneous alloys.J Non-Cryst Solids 2001;287:26–30.

[24] Safak M, Alper M, Kockar H.Parameters affecting microstructure and magnetoresistance of electrodeposited Co-Cu alloy films. J Magn Magn Mater 2006;784–6.

[25] Ben-Jacob E, Garik P. The formation of patterns in non-equilibrium growth.Nature 1990;343:523-30.

[26] Barkey DP. Structure and pattern formation in electrodeposition. In: Alkire RC, Kolb DM. eds. Advances in Electrochemical Science and Engineering, vol. 7, Wiley, New York, 2001, p. 151.

[27] Dick KA, Deppert K, Larsson MW, Martensson T, Seifert W, Wallenberg LR, Samuelson L. Synthesis of branched 'nanotrees' by controlled seeding of multiple branching events.Nat Mat 2004;3:380–4.

[28] Hermanson KD, Lumsdon SO, Williams JP, Kaler EW, Velev OD. Dielectrophoretic assembly of electrically functional microwires from nanoparticle suspensions.Science 2001;294:1082–6.

[29] Maksimovic VM, Lacnjevac UC, Stoiljkovic MM, Pavlovic MG, Jovic VD. Mater Charact 2012;62:1173–9.

[30] Czub J, Tokarz W, Gondek L, Figiel H. Interacting superparamagnetic nanoparticles in the Cu-1%Co single crystal.J Magn Magn Mater 2013;332:118–22.

[31] Nikolic ND, Popov KI, Pavlovic LJ, Pavlovic MG. Morphologies of copper deposits obtained by the electrodeposition at high overpotentials.Surf Coat Technol 2006;201:560–6.

[32] Ebadi M, Basirun WJ, Alias Y.Influence of magnetic field on the electrodeposition of Ni-Co alloy. J Chem Sci 2010;122(2):279–85.

[33] Li X, Ren Z, Fautrelle Y. Alignment behavior of the primary Al3Ni phase in Al-Ni alloy under a high magnetic field, J Crystal Grwth 2008;310:3488–97.

[34] Pamplin BR. Crystal Growth. Pergamon Press: Oxford, 1975.

[35] Franco V, Batlle X, Labarta A. CoFe-Cu granular alloys: From noninteracting particles to magnetic percolation.J Appl Phys 1999;85:7328-35.

[36] Gomez E, Labarta A, Llorente A, Valles E. Electrodeposited cobalt + copper thin films on ITO substrata.J Electroanal Chem 2001;517:63–8.

[37] Karaagac O, Kockar H, Alper M, Haciismailoglu M.Influence of Co:Cu ratio on properties of Co-Cu films deposited at different conditions. J Magn Magn Mater 2012;324:3834–8.

[38] Said AA; ElSalaam K, Hassan AMEA, Elawad AM,Elwahab MMMA. Effects of cobalt oxide iron oxide ratios on the catalytic activity of cobalt ferrite spinel catalysts.J Phys IV 1997;7:687–8.

[39] Chaudhari GN, Pawar MJ, Optoelectron O. Ethanol sensing performances of modified CoFe2O4 nanocrystals prepared by polymerizable complex route.Adv Mater 2008;10:2574–7.

[40] Sharma Y, Sharma N, Rao GVS, Chowdari BVR. Studies on spinel cobaltites, FeCo2O4 and MgCo2O4 as anodes for Li-ion batteries.Solid State Ionics 2008;179:587–97.

[41] Giri AK, Kirkpatrick EM, Moongkhamklang P, Majetich SA, Harris VG. Photomagnetism and structure in cobalt ferrite nanoparticles.Appl Phys Lett 2002;80:2341–3.

[42] Zhou JP, He HC, Nan CW. Effects of substrate temperature and oxygen pressure on the magnetic properties and structures of CoFe2O4 thin films prepared by pulsed-laser deposition.Appl Surf Sci 2007;253:7456–60.

[43] Sartale SD, Ganesan V, Lokhande CD.Electrochemical deposition and characterization of CoFe2O4 thin films.Phys Status Solidi A 2005;202:85–94.

[44] Araujo C, Almeida BG, Aguiar M, Mendes JA. Structural and magnetic properties of CoFe(2)O(4) thin films deposited by laser ablation on Si(001) substrates.Vacuum 2008;82:1437–40.

[45] Lokhande CD, Kulkarni SS, Mane RS, Nandi KC, Han SH.Structural and magnetic properties of single-step electrochemically deposited nanocrystalline cobalt ferrite thin films. Curr Appl Phys 2008;8:612–5.

[46] Hua ZH, Chen RS, Li CL, Yang SG, Lu M, Gu BX, Du YW. CoFe2O4 nanowire arrays prepared by template-electrodeposition method and further oxidization.J Alloy Compd 2007;427:199–203.

[47] Castaldi L, Giannakopoulos K, Travlos A, Niarchos D. Coevaporation of CoPt nanoparticles.Appl Phys Lett 2004;85:2854–6.

[48] He Z, Koza JA, Mu GJ, Miller AS, Bohannan EW, Switzer JA. Electrodeposition of CoxFe3-xO4 Epitaxial Films and Superlattices.Chem Mater 2013;25:223–32.

[49] Raoufi D. Morphological characterization of ITO thin films surfaces.App Surf Sci 2009;255:3682–6.

[50] Armyanov S. Crystallographic structure and magnetic properties of electrodeposited cobalt and cobalt alloys.Electrochim Acta 2000;3323–35.

[51] Li D, Daltin A-L, Wang Q, Chopart J-P, He J. The 9th International Pamir Conference on Fundamental and Applied MHD. Riga, Latvia, June 16–20,2014, Volume 2. pp. 179–183.